Chemical and Structural Characterization of the Interaction of Bleomycin A_2 with d(CGCGAATTCGCG)$_2$. Efficient, Double-Strand DNA Cleavage Accessible without Structural Reorganization

Michael V. Keck,[†] Richard A. Manderville,[‡] and Sidney M. Hecht*

Contribution from the Departments of Chemistry and Biology, University of Virginia, Charlottesville, Virginia 22901

Received October 27, 2000

Abstract: A detailed description of the interaction between Fe(II)·bleomycin A_2 and the Dickerson-Drew dodecamer d(CGCGAATTCGCG)$_2$ is presented. The reaction between bleomycin and this substrate leads to DNA cleavage at two major sites, adenosine$_5$ and cytidine$_{11}$, and two minor sites, cytidine$_3$ and thymidine$_8$. The pattern and relative intensities of cleavage at these sites was not entirely consistent with what would be predicted based on the preference of the drug for cleavage at the pyrimidines of 5′-GC-3′ and 5′-GT-3′ sites. Insight into the origins of the apparent alteration of selectivity was provided by examination of the structure of the duplex which had been determined by X-ray crystallography. This indicated that the C4′ hydrogens of the two nucleotides located at the strongest cleavage sites, C_{11} on one strand and A_5 on the other, were oriented toward each other in the minor groove. Two-dimensional NMR measurements and molecular dynamics modeling indicated that a metalloBLM could bind to the duplex in an orientation that positioned the metal center roughly equally close to each of these hydrogen atoms. On the basis of this observation, it was proposed that these two residues represented a double-stranded BLM cleavage site. This hypothesis was tested through the study of the BLM-mediated cleavage of the related decamer duplex, d(CGCGAATTCG)·d(CGAATTCGCG), as well as the hairpin sequence d(CGCGAATTCGIIIITTTTCCCCCGAATTCGCG). By the use of the hairpin oligonucleotide ^{32}P-labeled alternately at the 5′ and 3′-ends, unequivocal evidence was obtained for BLM-mediated double-strand cleavage. Quantitative analysis of the proportion of damage involving double-strand cleavage was effected by the use of the hairpin substrate; for damage initiated at the predominant cleavage site (cytidine$_{31}$, analogous to cytidine$_{11}$ in the dodecanucleotide), it is estimated that 43% of all damage leads to double-stranded lesions. The exceptional efficiency of double-strand cleavage observed in this system must reflect the spatial proximity and orientation of the two sugar H's whose abstraction is required to produce double-stranded lesions.

The bleomycins (BLM's, Figure 1) are a group of antitumor antibiotics that have been the subject of intensive investigations since their discovery in the mid 1960s.[1] The clinically used mixture, which consists primarily of BLM A_2 and BLM B_2, has found utility in the treatment of a variety of cancers, including non-Hodgkin's lymphoma, squamous cell carcinomas, and testicular tumors.[2] The therapeutic efficacy of BLM is believed to derive from its ability to bind to and oxidatively degrade cellular DNA,[3] and possibly RNA,[4] in the presence of certain metal ion cofactors, most notably iron.[5]

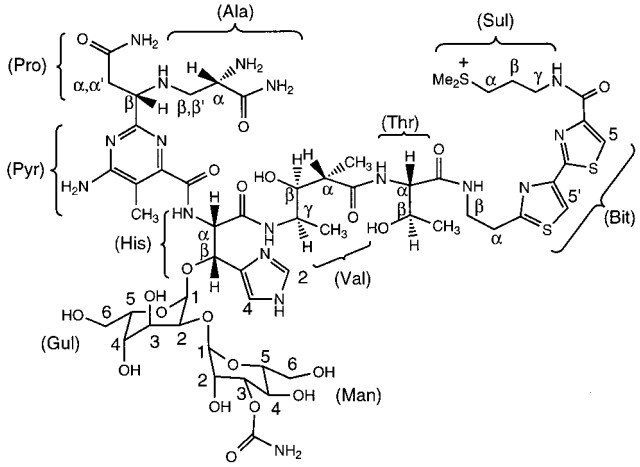

Figure 1. Structure of bleomycin A_2. The domains of the drug are indicated, as well as the designations for the protons observed during the NMR experiments.

The mechanism of BLM-mediated DNA cleavage has been studied in considerable detail. The process is initiated by abstraction of a hydrogen atom from the C4′ position of deoxyribose. DNA cleavage can then occur by either of two

* To whom correspondence should be addressed.

† Present address: Emporia State University, Emporia, Kansas.

‡ Present address: Wake Forest University, Winston-Salem, North Carolina.

(1) Umezawa, H.; Maeda, K.; Takeuchi, T.; Okami, Y. *J. Antibiot.* **1966**, *19A*, 200−209.

(2) (a) Umezawa, H. In *Bleomycin: Current Status and New Developments*; Carter, S. K., Crooke, S. T., Umezawa, H., Eds.; Academic Press: New York, 1978; pp 15−19. (b) *Bleomycin Chemotherapy*; Sikic, B. I., Rozencweig, M., Carter, S. K., Eds.; Academic Press: New York, 1985.

(3) (a) Stubbe, J.; Kozarich, J. W. *Chem. Rev.* **1987**, *87*, 1107−1136. (b) Natrajan, A.; Hecht, S. M. In *Molecular Aspects of Anticancer Drug−DNA Interactions*; Neidle, S., Waring, M. J., Eds.; Macmillan Press: London, 1993; pp 197−242. (c) Kane, S. A.; Hecht, S. M. *Prog. Nucleic Acid Res. Mol. Biol.* **1994**, 313−352. (d) Burger, R. M. *Chem. Rev.* **1998**, *98*, 1153−1169. (e) Claussen, C. A.; Long, E. D. *Chem. Rev.* **1999**, *99*, 2797−2816.

10.1021/ja003795i CCC: $20.00
Published on Web 08/18/2001

routes.[3] In an oxygen-dependent pathway, the deoxyribose radical combines with O_2 to form a C4′-peroxy radical. This reaction is the first in a series of steps which ultimately result in direct strand breakage and the production of 3′-termini having a phosphoroglycolate moiety.[6] Alternatively, under oxygen-deficient conditions, the deoxyribose radical can undergo transformation to the respective C4′−OH sugar[3] with subsequent elimination of free nucleobase from the intact strand and formation of an abasic site. Alkali treatment then leads to strand breakage and the formation of 3′-termini ending in phosphate or hydroxycyclopentenone moieties.[7]

For single-stranded DNA cleavage, which is the most prevalent and best studied event, BLM exhibits a strong preference for inducing oxidative damage at the pyrimidine moieties of 5′-GC-3′ and 5′-GT-3′ sequences.[8] However, BLM is also capable of effecting double-stranded DNA cleavage,[9] potentially a more lethal cellular event. BLM-mediated double-strand breakage has been shown to occur more frequently than would be expected for two independent but fortuitously close single-stranded cleavage events; it has, therefore, been thought that a single bound BLM molecule could be responsible for such lesions. Povirk and co-workers[10] have shown, based on the BLM-mediated cleavage of DNA restriction fragments, that double-strand cleavage occurs with different characteristics on both strands, in a fashion suggestive of an obligatory order of events. The putative primary (first) cleavage site is typically a 5′-GC-3′ or a 5′-GT-3′ site, while the secondary site on the opposite strand need not have this sequence. Direct strand scission must occur at the primary site via the C4′ peroxy radical intermediate for DNA modification to occur at the secondary site. Reaction at the secondary site can then occur via either of the two pathways described above. Povirk and co-workers found that the two sites involved in BLM-mediated double-stranded cleavage were either directly base paired or one base removed. These findings were substantiated by Absalon et al., using shorter hairpin substrates, although these latter studies did suggest a few possible mechanistic differences in the sequence of events.[11] Interestingly, in B-form DNA duplexes, the C4′ protons of two bases related in this manner are very far apart (>18 Å) and not oriented in the same direction. Thus, a significant structural rearrangement of the drug−DNA complex must be postulated; how this would be accomplished is not clear.

The structural basis for DNA binding interactions and the sequence selectivity of DNA cleavage by BLM have recently been studied through the use of one- and two-dimensional NMR spectroscopy.[12,13] Presently, we have focused our attention on the spectroscopically and crystallographically well-characterized Dickerson−Drew dodecamer, d(CGCGAATTCGCG)$_2$, which forms a self-complementary duplex whose structure is understood in detail both alone[14] and as a complex with low molecular weight ligands.[15] We report here a detailed study of the BLM-mediated cleavage of this substrate, which includes both single-stranded cleavage sites and a high-efficiency double-stranded cleavage site. By the use of one- and two-dimensional NMR experiments and molecular dynamics calculations, we have derived a structural model for BLM−DNA interaction. This model readily accommodates the observed biochemical transformations, and suggests a straightforward mechanism for double-stranded DNA cleavage.

Results

BLM-Mediated Cleavage of the Dodecanucleotide Substrate. The Dickerson−Drew dodecamer duplex, d(CGCGAATTCGCG)$_2$, was found to be a very efficient substrate for Fe(II)·BLM A_2-mediated degradation. As is clearly seen in Figure 2, two major cleavage sites were observed, occurring at positions A_5 and C_{11} (lane 2). In addition, longer incubation times resulted in the appearance of minor cleavage sites at T_8 and C_3 (vide infra). These major and minor sites are indicated by the solid and dashed arrows, respectively, in Figure 3a. As expected, piperidine treatment (lane 3) induced cleavage at abasic lesions formed during the BLM reaction, giving rise to (less mobile) products terminating at the 3′-end with either phosphate or hydroxycyclopentenone moieties.[7]

Two features of this experiment are particularly worthy of note. The first was the appearance of an anomalous low mobility band, clearly observed above the substrate band in lane 2 of Figure 2 and indicated in the figure by an asterisk (*). The appearance of a band at this position might be consistent with the formation of a covalent BLM−DNA cross-link, or might

(4) (a) Hecht, S. M. *Bioconj. Chem.* **1994**, *5*, 513−526. (b) Hecht, S. M. In *The Many Faces of RNA*; Eggleston, D. S., Prescott, C. D., Pearson, N. D., Eds.; Academic Press: London, 1998; pp 3−17. (c) Hecht, S. M. *J. Nat. Prod.* **2000**, *63*, 158−168.

(5) (a) Sausville, E. A.; Peisach, J.; Horwitz, S. B. *Biochem. Biophys. Res. Commun.* **1976**, *73*, 814−822. (b) Sausville, E. A.; Peisach, J.; Horwitz, S. B. *Biochemistry* **1978**, *17*, 2740−2745. (c) Sausville, E. A.; Stein, R. W.; Peisach, J.; Horwitz, S. B. *Biochemistry* **1978**, *17*, 2746−2754.

(6) (a) Burger, R. M.; Berkowitz, A. R.; Peisach, J.; Horwitz, S. B. *J. Biol. Chem.* **1980**, *255*, 11832−11838. (b) Giloni, L.; Takeshita, M.; Johnson, F.; Iden, C.; Grollman, A. P. *J. Biol. Chem.* **1981**, *256*, 8608−8615. (c) Uesugi, S.; Shida, T.; Ikehara, M.; Kobayashi, Y.; Kyogoku, Y. *Nucleic Acids Res.* **1984**, *12*, 1581−1592. (d) Sugiyama, H.; Ehrenfeld, G. M.; Shipley, J. B.; Kilkuskie, R. E.; Chang, L.-H.; Hecht, S. M. *J. Nat. Prod.* **1985**, *48*, 869−877. (e) Murugesan, N.; Xu, C.; Ehrenfeld, G. M.; Sugiyama, H.; Kilkuskie, R. E.; Rodriguez, L. O.; Chang, L.-H.; Hecht, S. M. *Biochemistry* **1985**, *24*, 5735−5744.

(7) (a) Burger, R. M.; Peisach, J.; Horwitz, S. B. *J. Biol. Chem.* **1982**, *257*, 8612−8614. (b) Wu, J. C.; Kozarich, J. W.; Stubbe, J. *J. Biol. Chem.* **1983**, *258*, 4694−4697. (c) Wu, J. C.; Kozarich, J. W.; Stubbe, J. *Biochemistry* **1985**, *24*, 7562−7568. (d) Wu, J. W.; Kozarich, J. W.; Stubbe, J. *Biochemistry* **1985**, *24*, 7569−7573. (e) Sugiyama, H.; Xu, C.; Murugesan, N.; Hecht, S. M. *J. Am. Chem.. Soc.* **1985**, *107*, 4104−4105. (f) Rabow, L. E.; Stubbe, J.; Kozarich, J. W.; Gerlt, J. A. *J. Am. Chem. Soc.* **1986**, *108*, 7130−7131. (g) Sugiyama, H.; Xu, C.; Murugesan, N.; Hecht, S. M.; van der Marel, G. A.; van Boom, J. H. *Biochemistry* **1988**, *27*, 58−67. (h) Rabow, L.; McGall, G. H.; Stubbe, J.; Kozarich, J. W. *J. Am. Chem. Soc.* **1990**, *112*, 3203−3208.

(8) (a) D'Andrea, A. D.; Haseltine, W. A. *Proc. Natl. Acad. Sci. U.S.A.* **1978**, *75*, 3608−3612. (b) Takeshita, M.; Grollman, A. P.; Ohtsubo, E.; Ohtsubo, H. *Proc. Natl. Acad. Sci. U.S.A.* **1978**, *75*, 5983−5987.

(9) (a) Suzuki, H.; Nagai, K.; Yamaki, H.; Tanaka, N.; Umezawa, H. *J. Antibiot.* **1969**, *22*, 446−448. (b) Mirabelli, C. K.; Ting, A.; Huang, C.-H.; Mong, S.; Crooke, S. T. *Cancer Res.* **1982**, *42*, 2779−2785.

(10) (a) Povirk, L. F.; Han, Y. H.; Steighner, R. J. *Biochemistry* **1989**, *28*, 5808−5814. (b) Steighner, R. J.; Povirk, L. F. *Proc. Natl. Acad. Sci. U.S.A.* **1990**, *87*, 8350−8354.

(11) (a) Absalon, M. J.; Kozarich, J. W.; Stubbe, J. *Biochemistry* **1995**, *34*, 2065−2075. (b) Absalon, M. J.; Wu, W.; Kozarich, J. W.; Stubbe, J. *Biochemistry* **1995**, *34*, 2076−2086.

(12) (a) Manderville, R. A.; Ellena, J. A.; Hecht, S. M. *J. Am. Chem. Soc.* **1994**, *116*, 10851−10852. (b) Manderville, R. A.; Ellena, J. A.; Hecht, S. M. *J. Am. Chem. Soc.* **1995**, *117*, 7891−7903. (c) Calafat, A. M.; Marzilli, L. G. *Comments Inorg. Chem.* **1998**, *20*, 121−141.

(13) Wu, W.; Vanderwall, D. E.; Stubbe, J.; Kozarich, J. W.; Turner, C. J. *J. Am. Chem. Soc.* **1994**, *116*, 10843−10844.

(14) (a) Drew, H. R.; Dickerson, R. E. *J. Mol. Biol.* **1981**, *151*, 535−556. (b) Patel, D. J.; Pardi, A.; Itakura, K. *Science* **1982**, *216*, 581−590. (c) Patel, D. J.; Ikuta, S.; Kozlowski, S.; Itakura, K. *Proc. Natl. Acad. Sci. U.S.A.* **1983**, *80*, 2184−2188. (d) Hare, D. R.; Wemmer, D. E.; Chou, S.; Drobny, G. J.; Reid, B. R. *J. Mol. Biol.* **1983**, *171*, 319−336. (e) Shui, X.; Sines, C. C.; McFail-Isom, L.; Van Derveer, D.; Williams, L. D. *Biochemistry* **1998**, *37*, 16877−16887. (f) Tereshko, V.; Minasov, G.; Egli, M. *J. Am. Chem. Soc.* **1999**, *121*, 470−471.

(15) (a) Patel, D. *Proc. Natl. Acad. Sci. U.S.A.* **1982**, *79*, 6424−6428. (b) Kopka, M. L.; Yoon, C.; Goodsell, D.; Pjura, P.; Dickerson, R. E. *Proc. Natl. Acad. Sci. U.S.A.* **1985**, *82*, 1376−1380. (c) Teng, M.; Usman, N.; Frederick, C. A.; Wang, A. H. *Nucleic Acids Res.* **1988**, *16*, 2671−2690. (d) Pelton, J. G.; Wemmer, D. E. *Biochemistry* **1988**, *27*, 8088−8096. (e) Lane, A. N.; Jenkins, T. C.; Brown, T.; Neidle, S. *Biochemistry* **1991**, *30*, 1372−1385. (f) Goodsell, D. S.; Kopka, M. L.; Dickerson, R. E. *Biochemistry* **1995**, *34*, 4983−4993.

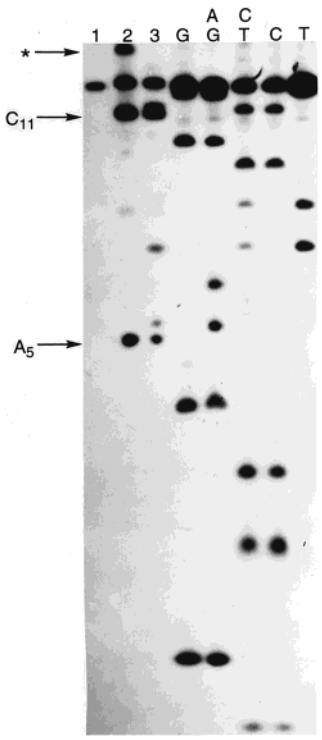

Figure 2. Products of the reaction of 20 μM Fe(II)·BLM A_2 with 6 μM 5′-^{32}P end labeled d(CGCGAATTCGCG)$_2$, analyzed by 20% sequencing polyacrylamide gel electrophoresis. Reactions were allowed to proceed for 30 min at 0 °C. Lane 1, DNA control; lane 2, DNA + Fe(II)·BLM A_2; lane 3, BLM reaction followed by piperidine treatment. Lanes marked G, AG, CT, C, and T indicate corresponding Maxam−Gilbert base specific reactions. The major cleavage sites are indicated to the left of the gel. The asterisk (*) denotes the anomalous low mobility product.

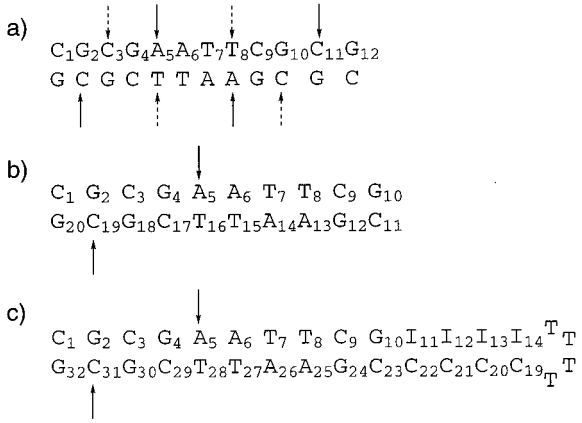

Figure 3. DNA substrates used in this study. Substrate b was a duplex formed from two decanucleotides. The major and minor sites of Fe·BLM-mediated cleavage are indicated by solid and dashed arrows, respectively.

be indicative of some other type of BLM-mediated DNA modification. Second, although both cytidine$_{11}$ and cytidine$_3$ represent prototypical 5′-GC-3′ BLM cleavage sites, only cytidine$_{11}$ was cleaved efficiently. Reaction at cytidine$_3$ was observed only at higher BLM concentrations (vide infra) or longer incubation times. Further, adenosine$_5$, which is present in a 5′-GA-3′ sequence context, was a very strong cleavage site. The intensity of cleavage at this site relative to both the C_{11} and C_3 sites was not anticipated. The basis for both of these observations was investigated in detail.

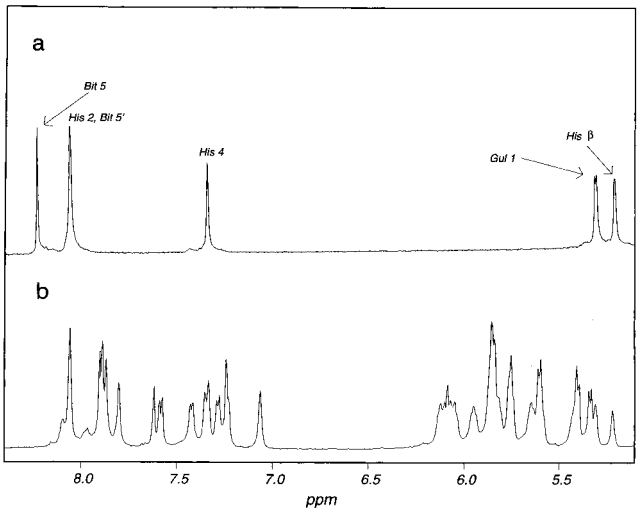

Figure 4. ^{1}H NMR spectra (5.1−8.4 ppm) of (a) Zn(II)·BLM A_2 and (b) a 1:1 complex of Zn(II)·BLM A_2 with the dodecanucleotide d(CGCGAATTCGCG)$_2$, in D_2O at 40 °C. Assignments of the β-hydroxyhistidine protons (His 2, His 4, His β), bithiazole protons (Bit 5, Bit 5′), and the gulose H1 proton (Gul 1) are indicated in part a.

Characterization of the Low-Mobility Product. Because a complete characterization of the BLM−dodecanucleotide reaction products was deemed essential to an understanding of the degradation of this substrate, the anomalous low-mobility band observed in Figure 2 was studied in detail. It was also of interest because of the possibility that the lesion represented a covalent BLM−DNA cross-link. Our characterization established that this band was due to the formation of a dodecanucleotide containing a BLM-generated abasic lesion at C_{11}, an observation that is not without precedent in BLM−DNA chemistry.[16] Details of this work can be found in the Supporting Information.

NMR Studies of the Zn·BLM−Dodecanucleotide Interaction. Shown in Figure 4 are one-dimensional ^{1}H NMR spectra (5.1−8.4 ppm) of Zn(II)·BLM A_2, both free and in the presence of 1 equiv of d(CGCGAATTCGCG)$_2$. Assignments of the proton resonances of the dodecamer and Zn·BLM A_2 in the 1:1 complex were obtained by analysis of NOESY and DQF-COSY spectra, essentially as described previously.[12a,b] Spectra were acquired both at 40 °C in the absence of added salt and at 15 °C in the presence of 40 mM NaCl. Previous assignments for all of the protons of the self-complementary dodecanucleotide[14c,d,17] and the Zn(II)·BLM A_2 complex[18] provided valuable guidance for the assignments made in this study.

The spectral changes that occurred upon addition of the dodecanucleotide to the Zn·BLM complex were similar to those observed upon binding of this complex to the self-complementary octanucleotide d(CGCTAGCG)$_2$.[12a,b] DNA−drug complex formation was indicated by the changes in the chemical shifts of the methyl valerate methyl groups (data not shown), and by the fact that the bithiazole aromatic protons (Bit 5, 5′) were not observed, presumably due to extensive line broadening.[12] In fact, these resonances could be observed only at temperatures above the DNA melting temperature of the 1:1 complex. As in the case of Zn·BLM binding to the octamer, no doubling of the

(16) Rabow, L. E.; Stubbe, J.; Kozarich, J. W. *J. Am. Chem. Soc.* **1990**, *112*, 3196−3203.
(17) Kellogg, G. W.; Schweitzer, B. I. *J. Biomol. NMR* **1993**, *3*, 577−595.
(18) (a) Oppenheimer, N. J.; Rodriguez, L. O.; Hecht, S. M. *Biochemistry* **1979**, *18*, 3439−3445. (b) Akkerman, M. A. J.; Haasnoot, G. A. G.; Hilbers, C. W. *Eur. J. Biochem.* **1988**, *173*, 211−225.

Table 1. Nonvicinal Intramolecular BLM−BLM NOE's and Intermolecular BLM−DNA NOE's in the Complex of Zn·BLM A_2 and d(CGCGAATTCGCG)$_2$

intramolecular BLM−BLM NOE's		intermolecular BLM−DNA NOE's	
His 2−Thr Me	Sul α−Sul γ	Sul α−C_1H5	Pro β −C_{11}H4′
His 4−Val Me	Bit NH−Thr β	Sul α−C_1H6	Ala β'−G_4H1′
His 4−Gul 1	Bit NH−Thr α	Sul β−C_1H6	Ala β'−G_4H4′
His 4−His β	Thr NH−Thr β	Bit α−G_{12}H1′	Ala α−G_4H1′
His β−Gul 1	Val NH−Val α	Bit β−C_{11}H1′	Ala α−G_4H4′
His β−Val Me	Val NH − Val β	Pro β−C_{11}H1′	Ala α−A_5H4′

DNA resonances was observed for the fully saturated complex, indicating that Zn(II)·BLM A_2 was in fast exchange ($>10^2$ s^{-1}) between the symmetry-related DNA binding sites.

Table 1 (Supporting Information) contains the ^{1}H shifts for Zn·BLM A_2, both free and when bound to the dodecanucleotide duplex (15 °C, 40 mM NaCl). For the free Zn·BLM complex, all proton resonances could be assigned from the DQF-COSY and NOESY spectra, acquired both in D_2O and in 9:1 H_2O−D_2O. In the DNA-bound complex, however, several of the gulose and mannose protons could not be assigned due to overlap with the H5′ and H5″ deoxyribose resonances. Additionally, the aromatic bithiazole protons (Bit 5, 5′) could not be detected, as noted above.

Inspection of Table 1 (Supporting Information) shows that chemical shift changes of the Zn·BLM A_2 resonances upon DNA binding were quite small ($\Delta\delta = |0.32|$ ppm). Nevertheless, some trends in the shifts can be noted. Protons of the metal binding domain tended to shift downfield (e.g., Ala α (+0.09 ppm), Pro α′ (+0.07 ppm), Pro β (+0.10 ppm)), while methylene protons of the bithiazole and sulfonium residues shifted upfield (Bit α (−0.15 ppm), Sul γ (−0.10 ppm)). The downfield shifts of the metal binding domain protons are consistent with minor groove binding, as these protons would be expected to interact with the edges of the DNA base pairs.[19] The upfield shifts of Bit α and Sul γ might reflect their positions between the stacked DNA bases.

Also apparent is the significant upfield shifting of the methyl valerate Hα proton (Val α (−0.18 ppm)). Upfield shifting of the Val α resonance has also been noted by Glickson and coworkers in their studies of Zn·BLM binding to poly(dA·dT).[20] This shift, however, rather than reflecting the position of this proton in the DNA base stack, might be indicative of a structural change in the BLM molecule upon DNA binding. Notable in this regard, the other Val protons (β and γ) were observed to shift downfield. Additionally, it is known that the Val α resonance of BLM A_2 is highly sensitive to complexation with the Zn^{2+} ion, but not to complexation with Cu^+ or Fe^{2+}. Specifically, Val α of metal-free BLM A_2 was found to resonate at 2.45 ppm in aqueous solution at 25 °C,[21] very similar to the corresponding resonances of 2.48 and 2.34 ppm for the Cu(I)[22] and the Fe(II)·CO[23] complexes, respectively. In contrast, the Val α resonance for the Zn(II) complex was located at 1.95 ppm (Supporting Information, Table 1). Oppenheimer and coworkers have shown[18a] that the shifting of Val α in the Zn(II)·BLM complex correlated with deprotonation of the imidazole ring of the β-hydroxyhistidine residue (His). Thus, binding of Zn(II)·BLM to DNA could enhance the interaction of Val α with the aromatic nucleus of the histidine ring by producing a more rigid Zn(II)·BLM structure.

The ^{1}H chemical shifts of the DNA resonances in the Zn·BLM−dodecamer complex are provided as Table 2 of the Supporting Information. Assignments of the individual DNA imino protons in H_2O were established by means of one-dimensional NOE experiments. These studies also permitted the unambiguous assignment of the base paired A_5 and A_6H2 protons, as these protons show strong NOE cross-peaks to the thymidine imino protons (data not shown).[14c] With the exception of several of the H5′ and H5″ DNA protons, the DNA proton chemical shifts could be assigned from the DQF-COSY and NOESY spectra. This task was facilitated in large part by the fact that, relative to the free dodecanucleotide, only small changes were noted. Virtually no change in the appearance of the DNA imino protons (not shown) was detected upon complexation with Zn(II)·BLM A_2, and examination of the DQF-COSY[24−27] and NOESY[28] spectra showed that the dodecanucleotide retained its B-form structure (see Supporting Information for details).

BLM-BLM and BLM-DNA NOEs. The structure of the free Zn·BLM A_2 complex was examined by 2D NMR at 15 °C, pH 7.0, both in D_2O and in 9:1 H_2O−D_2O. As observed previously,[18b] the NOESY spectra (τ_{mix} = 300 ms) displayed nonvicinal intramolecular NOE cross-peaks between protons of the metal binding domain and those of the methylvalerate residue. No cross-peaks were observed from the metal binding domain to protons from the threonine and bithiazole residues, a result which suggests that the free Zn(II)·BLM structure is extended, highly flexible, or both.[18b]

Upon DNA binding, an additional intramolecular NOE cross-peak between the H2 proton of the β-hydroxyhistidine unit (His 2) and the threonine methyl group (Thr Me) was noted, suggesting a folded BLM structure. This cross-peak was also detected for Zn(II)·BLM binding to the octanucleotide d(CGCTAGCG)$_2$,[12a,b] and has been noted for the free green Co(III)·BLM A_2 complex,[29] which is known to adopt a folded conformation. Further evidence for folding of the BLM structure was derived from the observation of intermolecular NOE contacts with the DNA that necessitated the close proximity of the functional domains of BLM.

At 15 °C, 12 intermolecular BLM−DNA cross-peaks could be detected for the Zn·BLM A_2−d(CGCGAATTCGCG)$_2$ complex (Table 1). These contacts are shown schematically in Figure 5, from which it is clear that they can be used to define the alignment of the drug as it resides on the duplex. An expanded portion of the NOESY spectrum (τ_{mix} = 300 ms) that highlights several of these intermolecular BLM-DNA cross-peaks is available as Figure 4 of the Supporting Information. Interestingly, the bithiazole Hα protons showed a cross-peak to G_{12}−H1′, while protons of the cationic tail showed cross-peaks to aromatic protons of C_1 (Sul α−C_1H5, C_1H6, Sul

(19) Wilson, W. D.; Li, Y.; Veal, J. M. *Adv. DNA Sequence Specific Agents* **1992**, *1*, 89.
(20) Glickson, J. D.; Pillai, R. P.; Sakai, T. T. *Proc. Natl. Acad. Sci. U.S.A.* **1981**, *78*, 2967−2971.
(21) Haasnoot, C. A. G.; Pandit, U. K.; Kruk, C.; Hilbers, C. W. *J. Biomol. Struct. Dyn.* **1984**, *2*, 449.
(22) Ehrenfeld, G. M.; Rodriguez, L. O.; Hecht, S. M.; Chang, C.; Basus, V. J.; Oppenheimer, N. J. *Biochemistry* **1985**, *24*, 81−92.
(23) Akkerman, M. A. J.; Neijman, E. W. J. F.; Wijmenga, S. S.; Hilbers, C. W.; Bermel, W. *J. Am. Chem. Soc.* **1990**, *112*, 7462−7474.
(24) (a) Haasnoot, C. A. G.; de Leeuw, F. A. A. M.; Altona, C. *Tetrahedron* **1980**, *36*, 2783−2792. (b) Van Wijk, J.; Huckriede, B. D.; Ippel, J. H.; Altona, C. *Methods Enzymol.* **1992**, *211*, 286−306.
(25) Bax, A.; Lerner, L. *J. Magn. Reson.* **1988**, *79*, 429−438.
(26) Nerdel, W.; Hare, D. R.; Reid, B. R. *Biochemistry* **1989**, *28*, 10008−10021.
(27) Schweitzer, B. I.; Mikita, T.; Kellogg, G. W.; Gardner, K. H.; Beardsley, G. P. *Biochemistry* **1994**, *33*, 11460−11475.
(28) Wuthrich, K. *NMR of Proteins and Nucleic Acids*; Wiley: New York, 1986.
(29) Xu, R. X.; Nettesheim, D.; Otvos, J. D.; Petering, D. H. *Biochemistry* **1994**, *33*, 907−916.

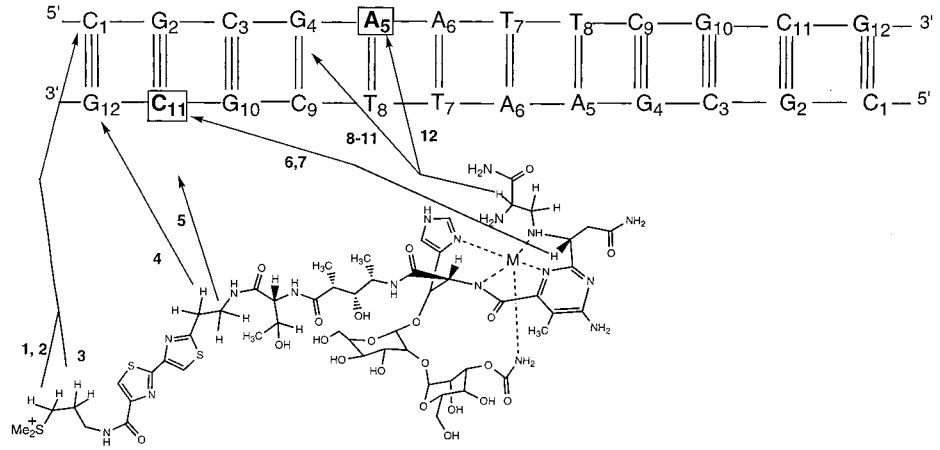

Figure 5. Schematic representation of the 12 intermolecular NOE contacts between Zn(II)·BLM A_2 and d(CGCGAATTCGCG)$_2$. Assignments: 1, Sul α−C_1H5; 2, Sul α−C_1H6; 3, Sul β−C_1H6; 4, Bit α−G_{12}H1′; 5, Bit β−C_{11}H1′; 6, Pro β−C_{11}H1′; 7, Pro β−C_{11}H4′; 8, Ala β′−G_4H1′; 9, Ala β′−G_4H4′; 10, Ala α−G_4H1′; 11, Ala α−G_4H4′; 12, Ala α−A_5H4′. The two major cleavage sites for Fe·BLM are boxed; the metal ion is denoted by M.

β−C_1H6). These contacts clearly established that the bithiazole moiety bound to the end of the dodecanucleotide, 3′ to the dominant C_{11} cleavage site. This observation is consistent with the lack of significant changes in the chemical shifts of the DNA protons upon Zn(II)·BLM binding, as the end of the helix in both the free and bound dodecanucleotide is likely to be poorly defined due to fraying.

Preference for localization of the metal binding domain near the C_{11} and A_5 residues was derived from the observation of intermolecular NOE cross-peaks connecting protons of the β-aminoalanine (Ala) and propionamide (Pro) residues with minor groove protons of G_4, A_5, and C_{11} (Table 1). Interestingly, the β-aminoalanine moiety of the drug is close to A_5H4′, the proton which is abstracted during cleavage, while the propionamide (Pro β) proton favors interactions with C4′−H of C_{11}. This observation indicates a preferred orientation of the metal binding domain within the minor groove binding site.

The intramolecular BLM−BLM and intermolecular BLM−DNA NOE cross-peaks that could be assigned for the Zn(II)·BLM−d(CGCGAATTCGCG)$_2$ complex are listed in Table 1. These cross-peaks were converted into distance ranges and were used as restraints to guide the molecular dynamics calculations.

Molecular Modeling. Modeling of the drug−DNA complex was carried out using the Insight II/Discover program. To model the BLM−metal ion interaction, five coordinate heme parameters within Insight II were utilized, as described previously.[12a,b] The d(CGCGAATTCGCG)$_2$ duplex was constructed in a standard canonical B-form. Using the NOE restraints listed in Table 1 to guide the molecular dynamics calculations on the entire drug−DNA complex, a model for the binding of Zn(II)·BLM A_2 to the duplex was determined. Listings of DNA−DNA restraints used in the calculations are available as Supporting Information (Tables 3 and 4).

Ten structures of the drug−DNA complex were generated using the modeling procedure described above and in the Experimental Section. Figure 6a shows a major groove view of a representative low-energy structure that satisfies all of the NOE restraints to within 0.2 Å. The bithiazole moiety is shown bound near the terminal DNA base pairs in a "trans" orientation. It is noteworthy that the bithiazole rings are not coplanar but rather exhibit a dihedral angle of 25°. The cationic sulfonium tail is positioned in the major groove. Since the terminal base pairs were constrained to be Watson−Crick hydrogen bonded in the modeling, the NOE restraints from the sulfonium tail of BLM to H5 and H6 of cytidine$_1$ necessarily represent major groove contacts. To satisfy these latter NOE contacts, the bithiazole moiety could in principle adopt any of several different binding modes, including intercalation, partial intercalation, or stacking at the end of the helix. All of these were represented in the 10 structures generated. Structures showing these alternative binding modes for the bithiazole moiety are available as Supporting Information (Figure 5).

Remarkably, in all 10 structures generated during the molecular dynamics calculations, the metal binding domain of BLM is positioned in approximately the same location in the minor groove of the helix, remaining indifferent to the exact nature of the DNA−bithiazole interaction. Hydrogen bonding contacts were generated from the pyrimidine NH_2 group and the primary amine of β-aminoalanine (indicated by yellow arrows in Figure 6a), as well as the amide group of propionamide (not shown), to the DNA phosphate and deoxyribose oxygens. These H-bonds apparently serve to anchor the metal binding domain in place. Figure 6b shows a minor groove view of the same structure, highlighting the orientation of the metal binding domain within the minor groove. From this view, it is clear that the metal ion (white ball) of the drug molecule is in relatively close proximity to both the C_{11}H4′ atom (6.4 Å, yellow ball) and the A_5H4′ atom of the opposite strand (5.4 Å, purple ball). The separations between these two protons in the 10 models generated ranged between 8.5 and 10.3 Å, indicating that the minor groove has widened somewhat to accommodate drug binding (compared to 5.0−5.5 and 8.3−9.0 Å at the two ends of the crystal structures of this duplex,[14a,e,f] and 5.8 Å in the computer-generated B-form DNA). This model suggests strongly that cleavage at either of the two major sites in this oligomer can be initiated by a single bound Fe(II)·BLM. Provocatively, it is consistent with the possibility that a single bound drug molecule could be responsible for a double-stranded cleavage event involving these two sites.

BLM-Mediated Cleavage of a Decanucleotide Related to the Dickerson Dodecanucleotide. The results of the structural studies described above prompted the examination of the reaction of BLM with the decanucleotide duplex d(CGCGAATTCG)·d(CGAATTCGCG), shown in Figure 3b. This duplex, which differs from the Dickerson dodecanucleotide only by the absence of two base pairs at one end, provided an unsymmetrical substrate in which each strand could be individually labeled

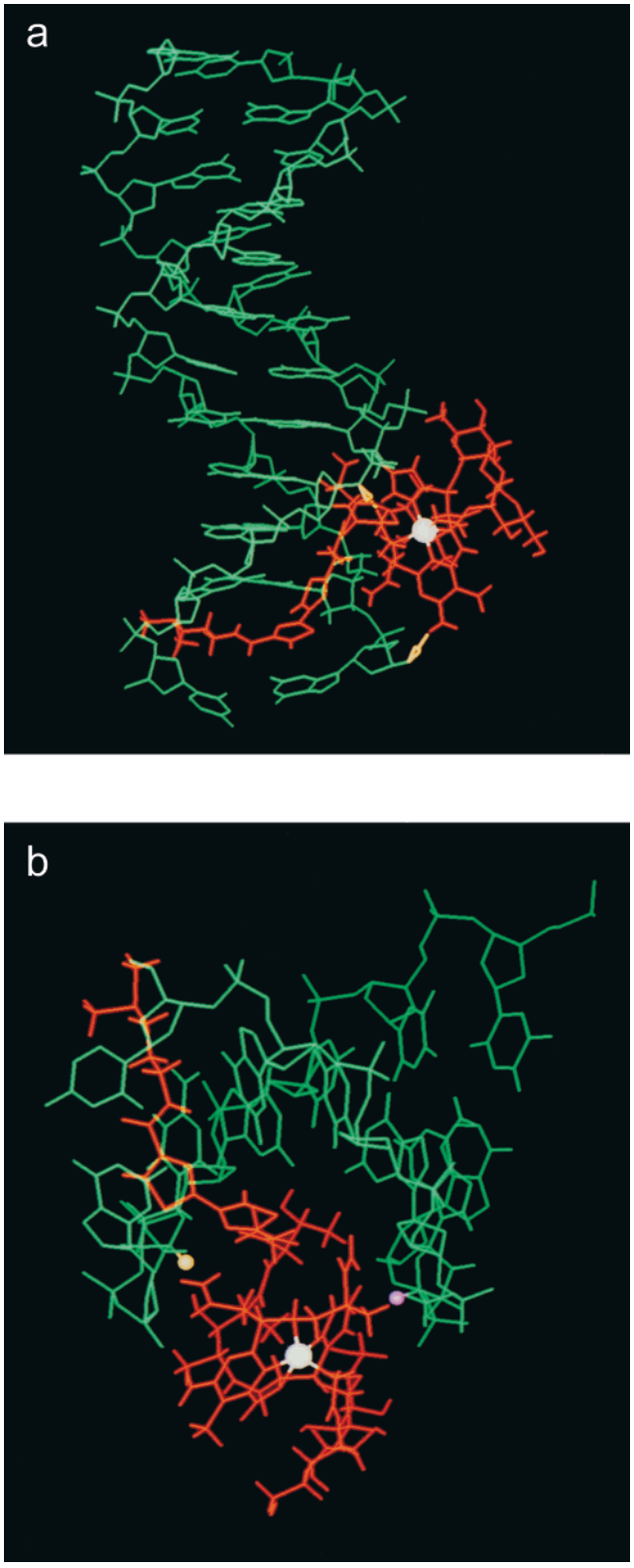

Figure 6. Model of the Zn(II)·BLM A_2−d(CGCGAATTCGCG)$_2$ complex determined by energy minimization and restrained molecular dynamics calculations. For clarity, hydrogen atoms are omitted from the DNA structure (green) but not from the Zn(II)·BLM A_2 model (red). (a) Major groove view (top). Perspective highlighting the orientation of the BLM relative to the duplex. Hydrogen bonding contacts from the pyrimidine NH_2 group and the primary amine of β-aminoalanine to the DNA ribose and phosphate oxygens are shown as yellow arrows. The metal ion of BLM is indicated by the white ball. (b) Minor groove view (bottom). Perspective looking into the minor groove of the dodecanucleotide. The metal ion lies 6.4 Å from C_{11}H4′ (yellow ball) and 5.4 Å from A_5H4′ (purple ball) on the opposite strand.

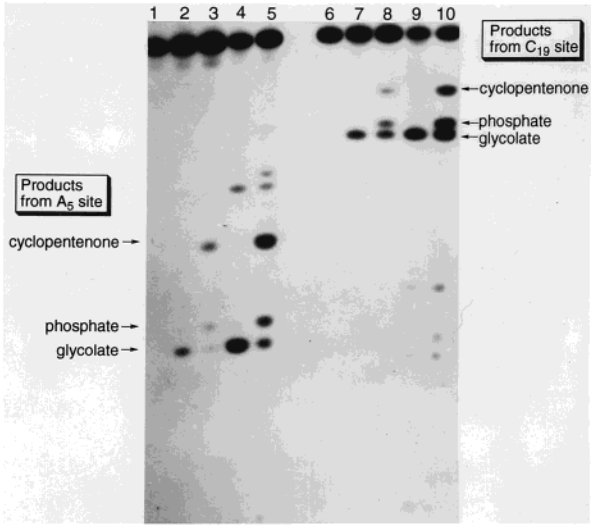

Figure 7. Products of the reaction of Fe(II)·BLM A_2 with 1 μM decanucleotide duplex d(CGCGAATTCG)·d(CGAATTCGCG), analyzed by 20% sequencing polyacrylamide gel electrophoresis. Reactions were allowed to proceed for 30 min at 0 °C. Lanes 1−5 illustrate cleavage of the top strand as defined in Figure 3b, while lanes 6−10 illustrate cleavage of the bottom strand. Lane 1, 5′-^{32}P end labeled top strand control; lane 2, DNA + 10 μM Fe(II)·BLM A_2; lane 3, 10 μM Fe(II)·BLM A_2, followed by treatment with *n*-butylamine; lane 4, DNA + 25 μM Fe(II)·BLM A_2; lane 5, 25 μM Fe(II)·BLM, followed by treatment with *n*-butylamine; lane 6, 5′-^{32}P end labeled bottom strand control; lane 7, DNA + 10 μM Fe(II)·BLM A_2; lane 8, 10 μM Fe(II)·BLM A_2, followed by treatment with *n*-butylamine; lane 9, DNA + 25 μM Fe(II)·BLM A_2; lane 10, 25 μM Fe(II)·BLM, followed by treatment with *n*-butylamine. Cleavage products for the major cleavage site on each strand are indicated.

and analyzed. In addition, it eliminated one of the C_{11} cleavage sites, but not the A_5 to which it was putatively coupled.

The cleavage of each strand of this decanucleotide duplex in the presence of 10 and 25 μM concentrations of Fe(II)·BLM A_2 is shown in Figure 7. Importantly, each strand exhibited only one major cleavage site. The top strand was cleaved primarily at position A_5, while the bottom strand showed cleavage almost exclusively at C_{19} (the position equivalent to C_{11} in the dodecanucleotide), as indicated by the arrows in Figure 3b. At the lower Fe(II)·BLM concentration, these were the only cleavage sites observed, although at the higher concentration other weak sites appeared, as were seen with the dodecanucleotide (vide supra). Significantly, no cleavage was observed at A_{13} in the bottom strand. This result supports the hypothesis that C_{11} and A_5 (in the dodecanucleotide numbering scheme) are coupled in a BLM-mediated double-stranded DNA cleavage event.

Treatment of these reaction mixtures with 0.2 M *n*-butylamine afforded additional products due to alkali cleavage at the BLM-induced abasic lesions, as expected.[7g,30] Two additional bands were observed, corresponding to 3′-ends terminating in phosphate and in hydroxycyclopentenone,[7e,g] as indicated in lanes 3, 5, 8, and 10 of Figure 7. Phosphorimager analysis was used to determine the relative amounts of alkali-labile lesion (phosphate and hydroxycyclopentenone) and frank strand scission (glycolate) obtained for each of the two cleavage sites. The results, shown in Table 2, indicated that both sites afforded greater than 50% alkali-labile lesion, an observation not typical of a single-stranded cleavage event. Cleavage of the octanucleotide sequence d(CGCTAGCG)$_2$, a well-studied substrate in this

(30) Aso, M.; Kondo, M.; Suemune, H.; Hecht, S. M. *J. Am. Chem. Soc.* **1999**, *121*, 9023−9033.

Table 2. Partitioning of the Decanucleotide and Octanucleotide DNA Modification Events between Direct Strand Scission and Abasic Site Formation[a]

	decanucleotide		
	top strand (A_5)	bottom strand (C_{19})	octanucleotide (C_7)
cyclopentenone	63%	26%	20%
phosphate	20%	33%	20%
glycolate[b]	17%	41%	60%

[a] Results are the averages of three experiments. [b] Product resulting from direct strand scission.

laboratory,[31] afforded ~60% direct strand scission (data not shown). In contrast, the C_{19} site in this decanucleotide substrate afforded 41% glycolate, while the A_5 site afforded only 17% glycolate. Also notable was the difference in the ratio of strand scission:alkali-labile lesion formed at these two sites. The C_{19} site was clearly much more prone to direct strand scission than was A_5.

BLM-Mediated Cleavage of a DNA Hairpin Substrate. As a further test of the facility of BLM-mediated double-stranded cleavage involving these two sites, a 32-nucleotide hairpin substrate (Figure 3c) was studied. This oligonucleotide was shown by nondenaturing PAGE in comparison with appropriate reference duplexes to form hairpin sequences under the conditions employed (data not shown). It was then ^{32}P end labeled at either the 5′- or 3′-end and allowed to react with Fe(II)·BLM A_2. The results are shown in Figure 8. Figure 8a shows the cleavage of the 5′-^{32}P end labeled substrate at a range of BLM concentrations spanning 1−10 μM. Two major cleavage sites were observed. One of these corresponded to A_5, a site involved in the putative double-stranded cleavage event. Surprisingly, the second strong cleavage site occurred at I_{11}, the first inosine of the linker region. Notably, minimal cleavage was observed at C_{31}, the position that corresponds to C_{11} in the dodecanucleotide.

Parallel results were observed for the 3′-^{32}P end labeled substrate, as shown in Figure 8b. A single strong cleavage site was observed at C_{31}, along with some weaker ones. The A_5 site, which was very strong for the 5′-labeled substrate, was only faintly observed for the 3′-labeled oligomer. This result has strong implications for the existence of a double-stranded cleavage site, as discussed below.

Also of note for this substrate was the observation of a cleavage site at C_{22}, the nucleotide base paired to the strongly cleaved I_{11} site. Together, the cleavage observed at these two sites (I_{11} and C_{22}) parallels very closely the characteristics of a double-stranded cleavage site as defined previously[10,11] and may represent such a site, although a detailed characterization of this possible double-strand cleavage site was not pursued.

Phosphorimager analysis of the gels in Figure 8, as well as those from experiments in which the BLM reaction was followed by alkali treatment (data not shown), was carried out to characterize the cleavage observed at C_{31} and A_5 in a more quantitative fashion. For cleavage of the DNA by 10 μM Fe(II)·BLM A_2, the amount of damage at C_{31} (derived from both single- and double-stranded events) was determined from the 3′-^{32}P end labeled substrate to be 11.8% of the total DNA in the lane: 7.6% from frank strand scission and 4.2% from abasic site formation. This corresponds to a 65:35 glycolate−abasic lesion ratio. Additionally, from the gel containing the 5′-^{32}P end labeled substrate, direct single-strand cleavage at C_{31} was observed to account for 2.6% of the total DNA in the lane. Similarly, DNA modification at A_5 was found, by quantification of cleavage of the 5′-^{32}P end labeled substrate, to yield a glycolate−phosphate ratio of 31:69 (A_5 damage accounts for 20% of total DNA in the lane). From the 3′-^{32}P end labeled fragment, it was found that single-stranded cleavage at A_5 accounted for only 1% of the total DNA.

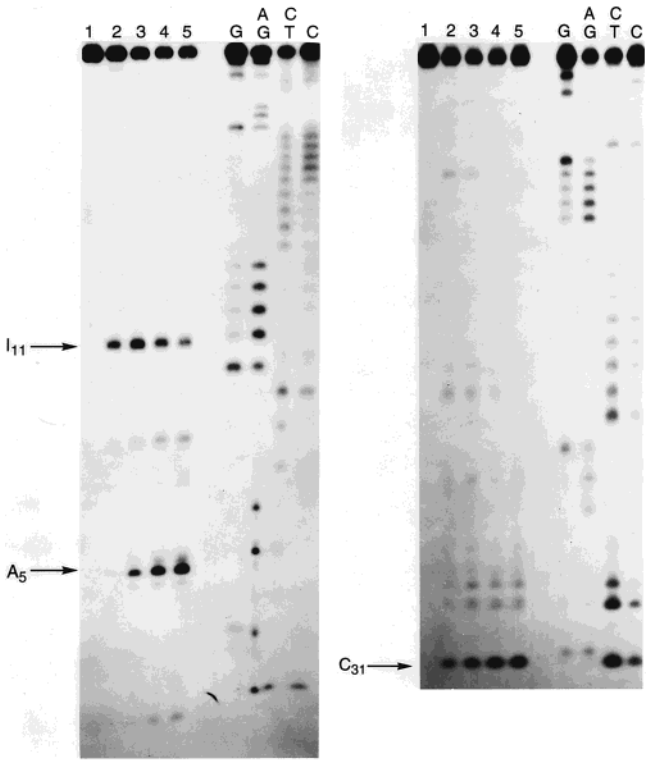

Figure 8. Products of the reaction of Fe(II)·BLM A_2 with (a, left) 5′-^{32}P end labeled and (b, right) 3′-^{32}P end labeled hairpin substrate shown in Figure 3c. Reactions were allowed to proceed for 20 min at 0 °C. (a) Lane 1, 5′-^{32}P end labeled hairpin control; lane 2, DNA + 1 μM Fe(II)·BLM A_2; lane 3, DNA + 2 μM Fe(II)·BLM A_2; lane 4, DNA + 5 μM Fe(II)·BLM A_2; lane 5, DNA + 10 μM Fe(II)·BLM A_2. (b) Lane 1, 3′-^{32}P end labeled hairpin control; lane 2, DNA + 1 μM Fe(II)·BLM A_2; lane 3, DNA + 2 μM Fe(II)·BLM A_2; lane 4, DNA + 5 μM Fe(II)·BLM A_2; lane 5, DNA + 10 μM Fe(II)·BLM A_2. Lanes marked G, A+G, C+T, and C indicate the corresponding Maxam−Gilbert base specific reactions.

Discussion

Although the interaction of BLM with DNA has been studied for a number of years, the factors that lead to DNA binding selectivity, as well as those that direct sequence specificity of cleavage, are still poorly understood.[3] To gain insight into the structural basis of these phenomena, we studied the interaction of BLM with the structurally well-defined Dickerson−Drew dodecanucleotide from both biochemical and structural perspectives. This substrate contains two 5′-GC-3′ sites, which are known to be favorable sites for BLM-induced DNA damage. It additionally contains a central −AT− rich region, such as those known to bind preferentially to bithiazoles.[32]

Cleavage of this substrate by Fe(II)·BLM provided some surprises. In addition to four cleavage products, an anomalously slow migrating band was observed by PAGE. Such bands are often indicative of covalent drug−DNA cross-links.[33] No report

(31) Van Atta, R. B.; Long, E. C.; Hecht, S. M.; van der Marel, G. A.; van Boom, J. H. *J. Am. Chem. Soc.* **1989**, *111*, 2722−2724.

(32) (a) Quada, J. C., Jr.; Zuber, G. F.; Hecht, S. M. *Pure Appl. Chem.* **1998**, *70*, 307−311. (b) Zuber, G.; Quada, J. C., Jr.; Hecht, S. M. *J. Am. Chem. Soc.* **1998**, *120*, 9368−9369.

has appeared, however, that demonstrates well-characterized BLM−DNA adducts of this type; in fact, further analysis of this product demonstrated that it was derived from an abasic lesion at the C_{11} position of the oligonucleotide. Notably, other reports describing the reactions of oxidative DNA damaging agents with DNA have also documented similar slow migrating bands. Examples include the reaction of Fe(II)·BLM with $tRNA^{Phe34}$ and the reaction of hairpin deoxyribonucleotide substrates with Ni(II)(SALEN) derivatives.[35] While subsequent studies of the latter system do provide support for the existence of a covalent DNA adduct,[36] the results reported here raise the possibility that apparent adducts, for which no detailed chemical characterizations have been reported, may actually represent abasic sites.

The relative intensities of the cleavage products is also notable. The major cleavage sites were found to be A_5 and C_{11}. While C_{11} was expected from sequence context to be strongly targeted by Fe(II)·BLM A_2, the intensity of the cleavage at A_5 was striking. Further, even though C_3 was also present in a −GC− sequence context, cleavage at this site was quite weak. To understand these unanticipated results, we used molecular dynamics simulations, guided by NOE-derived distance constraints, to generate models for BLM−duplex interaction.

The NMR experiments exhibited features that were in many respects similar to those observed for the Zn(II)·BLM−d(CGCTAGCG)$_2$ complex described previously.[12a,b] Binding of the drug to the DNA does not abolish the 2-fold symmetry of the duplex, implying that exchange between symmetry-related sites is fast on the NMR time scale. Further, the extensive line broadening of the bithiazole region suggests that this domain of BLM undergoes rapid exchange between magnetically inequivalent sites. The observed NOE cross-peaks, both inter- and intramolecular, were used to derive the distance constraints employed during the molecular dynamics simulations. It should be noted that symmetry was not imposed during the modeling, and that the 10 structures generated are in rapid equilibrium with those that involve Zn(II)·BLM binding to the 2-fold symmetric sites. Further, it should be noted that utilizing structural studies of Zn(II)·BLM as the basis for explaining the structural and biochemical behavior of Fe(II)·BLM may be difficult due to a number of ambiguities in our understanding of the relationship between these two metallobleomycins.[12a,b]

Ten structures with similar energies were generated; a representative model is shown in Figure 6. All 10 structures placed the bound bithiazole moiety at the end of the helix, rather than at the −AT− rich center. This location was derived from intermolecular NOE contacts from protons of the sulfonium tail and the peptide linker to the DNA. However, considerable variation occurred in the modes of binding of the bithiazole, which included intercalation, partial intercalation, and stacking at the end of the helix (alternative structures are available as Supporting Information, Figure 5). The NMR data were not conducive to localization of these rings, as the ring protons were not observable and thus showed no intermolecular NOE contacts. Such a result is not surprising, given that the ends of oligonucleotides tend to fray in solution. The fact that the bithiazole moiety binds at the end of the helix precludes a quantitative description of its binding mode. It is not unlikely that a mixture of different bithiazole orientations is present, all of which lend significant binding energy to the drug−DNA complex.

In contrast to the bithiazole, several key intermolecular NOE contacts between the DNA and metal-binding domain of BLM were observed. In fact, all 10 of the generated models placed this domain in approximately the same location and orientation in the minor groove of the helix. A minor groove view of the complex highlighting the metal-binding domain is shown in Figure 6b. The dominant feature of this model is the proximity of the metal center of BLM to the C4′ protons of both the C_{11} residue (6.4 Å) and the A_5 residue on the opposite strand (5.4 Å). The two hydrogen atoms are themselves separated by 9.6 Å in the structure shown; in the 10 structures generated, this distance ranged from 8.5 to 10.3 Å. These distances are slightly larger than those measured for the free dodecanucleotide duplex (5−9 Å),[14a,e,f] an indication that the minor groove widens appreciably to accommodate binding of the metal complex.[12b]

From this model, the origin of the observed cleavage specificity is clear. The predominant binding configuration of the drug−DNA complex places the metal center in a position such that the C4′ hydrogens of the C_{11} and A_5 nucleotides are readily and approximately equally accessible. In contrast, the analogous hydrogen atom on the C_3 residue is not as accessible. In the structure presented in Figure 6, C_3H4′ lies 12.2 Å from the metal center (an average of 12.3 Å in the 10 structures generated) and is oriented away from it. This hydrogen is thus not readily accessible to BLM bound as indicated by the NMR measurements, even though significant cleavage at C_3 might be expected from sequence context.[3,37]

It may be worth noting in this context that the self-complementary oligonucleotide d(CGCT$_3$A$_3$GCG)$_2$ was cleaved predominantly (85:15) at C_{11} rather than C_3[37] by Fe(II)·BLM A_2, and that a similar cleavage ratio favored C_7 relative to C_3 in d(CGCTAGCG).[31] That these two sites were cleaved in independent events is suggested strongly by the alteration in C_3/C_{11} cleavage ratio[37] and C_3/C_7 DNA binding characteristics noted for deglycoBLM A_2 using these same two substrates.

In addition to providing a structural basis for the observed cleavage specificity of this duplex, the model further suggests that this binding site is geometrically predisposed for a double-stranded cleavage event involving the C_{11} and A_5 residues. Double-stranded oxidative DNA cleavage creates damage that, for obvious reasons, might be considered much more difficult for a cell to repair. Thus, double-strand cleavage has been proposed to be of importance therapeutically.[38] BLM-mediated double-strand DNA cleavage is believed to account for approximately 10% of all DNA damage caused by the drug. Although a double-strand break could in principle originate either from a single bifunctional cleavage event or from two coincidentally close single-stranded events, early evidence demonstrated that double-strand breaks occurred under conditions of single-hit kinetics. Further, the extent of such cleavage was too great statistically to result from two coincidentally close single-stranded cleavage sites.[39] These observations, however, presented an interesting dilemma, as the mechanistic pathway

(33) (a) Weidner, M. F.; Sigurdsson, S. T.; Hopkins, P. B. *Biochemistry* **1990**, *29*, 9225−9233. (b) Armstrong, R. W.; Salvati, M. E.; Nguyen, M. *J. Am. Chem. Soc.* **1992**, *114*, 3144−3145. (c) Lee, C.; Gibson, N. W. *Biochemistry* **1993**, *32*, 2592−2600.

(34) Hüttenhofer, A.; Hudson, S.; Noller, H. F.; Mascharak, P. K. *J. Biol. Chem.* **1992**, *267*, 24471−24475.

(35) Muller, J. G.; Paikoff, S. J.; Rokita, S. E.; Burrows, C. J. *J. Inorg. Biochem.* **1994**, *54*, 199−206.

(36) Stemmler, A. J.; Burrows, C. J. *J. Am. Chem. Soc.* **1999**, *121*, 6956−6957.

(37) Sugiyama, H.; Kilkuskie, R. E.; Chang, L.-H.; Ma, L.-T.; Hecht, S. M.; van der Marel, G. A.; van Boom, J. H. *J. Am. Chem. Soc.* **1986**, *108*, 3852−3854.

(38) Povirk, L. F. In *Molecular Aspects of Anti-cancer Drug Design*; Neidle, S., Waring, M., Eds.; MacMillan: London, 1983; pp 157−181.

(39) Povirk, L. F.; Wübker, W.; Köhnlein, W.; Hutchinson, F. *Nucleic Acids Res.* **1977**, *4*, 3573−3580.

by which BLM was believed to function did not obviously provide for bifunctionality.

Over the past decade, the characteristics of double-stranded cleavage have been described in greater detail. On the basis of analyses of the reactions of Fe(II)·BLM with DNA restriction fragments, Povirk and co-workers[10,40] have suggested that double-strand cleavage is initiated by C4′-hydrogen abstraction at a −GC− or −GT− site, termed the primary site, in a process similar to that observed for single-strand cleavage. For subsequent double-strand cleavage to occur, the C4′ radical produced must combine with molecular oxygen, the first committed step on the pathway leading to direct strand scission, to form a C4′-peroxy radical intermediate. The peroxy radical then must regenerate activated BLM, which can subsequently proceed to abstract the C4′-hydrogen from the secondary site and initiate cleavage via either the oxygen-dependent or oxygen-independent pathway.[3,6,7] This secondary site was always either directly base-paired to or one base pair removed from the primary site, and it rarely fit the preferred 5′-G-pyrimidine-3′ sequence. Further, single-stranded cleavage at this secondary site was never observed.

This hypothesis was generally supported by the recent reports of Absalon et al., who carried out a detailed mechanistic study using hairpin oligonucleotide substrates.[11] These authors further provided a mechanism, based on their own work and that of Povirk, that accommodated both cleavage and metal center reactivation. This mechanism was fully consistent with all of the data. Nonetheless, while these studies leave little doubt that double-strand cleavage is a significant aspect of BLM activity, the model is still complex from a structural viewpoint. As noted,[11b] the primary and secondary sites are disposed such that the C4′-hydrogens are separated by a distance of greater than 18 Å and are directed away from each other. For double-strand cleavage to occur, a significant reorientation of either the drug or the DNA substrate must, therefore, occur on a time scale that is faster than both the lifetime of activated BLM and the dissociation rate of BLM from the DNA. While this reorganization has recently been proposed to occur based on molecular modeling,[41] the precise molecular mechanism(s) is unclear at present.

The model presented in this paper describes a geometrically simpler double-strand cleavage site. No reorientation is required to allow access of the metal to both hydrogens. To verify chemically that the C_{11}/A_5 couple actually represented such a double-strand cleavage site, derivatives of the dodecanucleotide were studied. Reactions of Fe(II)·BLM A_2 with the decanucleotide (Figure 3b) and the hairpin (Figure 3c) gave results that were fully consistent with the double-strand cleavage hypothesis. Specifically, the decanucleotide substrate was designed such that the C_{11} residue was absent from one end of the duplex. As expected, removal of this C_{11} site also eliminated cleavage at the "A_5" site to which it was putatively coupled in a double-strand cleavage site. Cleavage occurred only at the "C_{11}" (C_{19}) and A_5 sites of the unaltered end of the decanucleotide. This result argues that both the C_{11} and A_5 sites are cleaved by the same bound BLM molecule and provides support for their involvement in a double-strand cleavage event.

The product ratios resulting from cleavage at these sites were also shown to differ from those characteristic of single-strand cleavage sites, i.e., in terms of the relative amounts of strand scission products and abasic lesions formed. The C_{19} and A_5 sites afforded 41 and 17% glycolate, respectively, as listed in Table 2, compared to the 60−70% normally observed for a single-strand event.[3,6,7,42] The reason for the abnormally high percentage of alkali-labile lesion formed during the cleavage of this substrate is not understood definitively in mechanistic terms although an analogous observation has been made for a methylated DNA oligonucleotide substrate.[43] However, the greater amount of glycolate at C_{19} relative to that formed at A_5 is consistent with the former site being the primary one in a sequential process, as direct strand scission would be required at this site (and only this site) according to the mechanism suggested by Povirk.[10,40]

Unequivocal evidence for a double-strand cleavage event involving these two sites derived from the study of the hairpin substrate (Figure 3c). It contains a 14 base pair stem which incorporates the decanucleotide duplex sequence described above connected to a $d(T)_4$ loop via a $d(I{\cdot}C)_4$ linker. The linker was designed to keep the loop spatially removed from the decanucleotide region and thus minimize any structural effects that it might cause; such effects were significant for several other hairpins studied (data not shown). Treatment of the 5′ ^{32}P-end labeled hairpin oligonucleotide with Fe(II)·BLM A_2 revealed strong cleavage at A_5, but only very weak cleavage at C_{31}. Alternatively, the 3′ ^{32}P-end labeled substrate revealed strong cleavage at C_{31}, but only weak cleavage at A_5. If the cleavage observed at these two sites had involved independent single-stranded events, their observed relative intensities should have been the same regardless of the position of radiolabeling. In a reaction involving coupled cleavage on both strands, however, analysis by gel electrophoresis would reveal only the site nearest the ^{32}P-end label; fragments resulting from cleavage at the remote site would contain no ^{32}P-end label and would not be observed. This is essentially what was found to occur for the differentially ^{32}P-end labeled hairpins studied here. Strong cleavage was apparent only at the site nearest the label. This result is possible only if both strands are being cleaved in a coordinated process. These experiments, therefore, provide unequivocal evidence that C_{31} and A_5 represent a double-strand DNA cleavage site. Importantly, however, it should be noted that because small amounts of cleavage are observed at the sites remote from the ^{32}P label, limited single-strand cleavage must also be occurring at each site. Further, the method of analysis permits direct measurement of the extent of single-strand cleavage at each site.

From phosphorimager analysis of the gels shown in Figure 8, as well as similar gels in which base treatment was carried out after the BLM reaction, an estimate for the partitioning between single- and double-strand cleavage involving C_{31} was made. For this purpose, it was assumed, as per the analysis provided by Povirk and co-workers,[10,40] that C_{31} was the primary site of oxidative DNA damage and that all double-strand cleavage initiated at this site via the pathway involving a C-4′ hydroperoxynucleotide intermediate. The first assumption is supported by the studies of the decanucleotide duplex and by the observation that single-strand cleavage at C_{31} is 2.6 times more prevalent than single-strand cleavage at A_5 (vide supra). The validity of the second assumption has been recently substantiated by Absalon et al. through studies of double-strand cleavage under oxygen-deficient conditions.[11b]

(40) Povirk, L. F.; Houlgrave, C. W. *Biochemistry* **1988**, *27*, 3850−3857.

(41) (a) Vanderwall, D. E.; Lui, S. M.; Wu, W.; Turner, C. J.; Kozarich, J. W.; Stubbe, J. *Chem. Biol.* **1997**, *4*, 373−387. (b) Hoehn, S.; Junker, H.-D.; Kozarich, J.; Turner, C.; Stubbe, J. American Chemical Society Meeting, 1999; Abstracts, 311-MEDI. (c) Hoehn, S. T.; Junker, H.-D.; Bunt, R. C.; Turner, C. J.; Stubbe, J. *Biochemistry* **2001**, *40*, 5894−5905.

(42) Sugiyama, H.; Kilkuskie, R. E.; Hecht, S. M. *J. Am. Chem. Soc.* **1985**, *107*, 7765−7767.

(43) Long, E. C.; Hecht, S. M.; van der Marel, G. A.; van Boom, J. H *J. Am. Chem. Soc.* **1990**, *112*, 5272−5276.

From these data, it was determined that cleavage at C_{31}, mediated by the presence of 10 μM Fe(II)·BLM A_2, resulted in a glycolate:alkali-labile lesion ratio of 65:35 (7.6% glycolate: 4.2% abasic site, vide supra), a value that is somewhat different than that observed for the decanucleotide duplex, but one that is more typical of BLM−DNA reactions with other DNA oligonucleotide substrates.[6,7,42] It follows that 65% of the damage occurring at C_{31} could potentially lead to double-stranded DNA cleavage. However, a partitioning between single-strand and double-strand cleavage events should be expected. This partitioning presumably depends to a significant extent on the efficiency of BLM reactivation, the determining factors of which are unknown. The actual amount of single-stranded cleavage at C_{31} could be determined directly from the intensity of the band at this site in the 5′ ^{32}P-end labeled substrate; it represented 2.6% of the total DNA. Therefore, 34% of the total glycolate produced (2.6/7.6) is derived from single-strand cleavage at this site. Accordingly, ∼43% (i.e. 0.66 × 0.65) of all DNA damage initiated at C_{31} leads to double-strand lesions.

For a set of internally labeled hairpin substrates, Absalon et al.[11a] observed ratios of single-strand to double-strand cleavage of between 3.3 and 5.8. These data indicate that appoximately 15−25% of the cleavage observed at the primary site was part of a double-strand cleavage event. Since these studies failed to account for the production of abasic lesions, the actual percentage of double-strand modification relative to both types of potential DNA damage is probably somewhat different. For the purpose of comparison, we assume a partitioning of glycolate: alkali labile lesion equal to 65:35 in their system. On the basis of this assumption, we estimate that ∼15−20% of the damage initiated at the primary site was involved in double-strand DNA chemistry. In contrast, the double-strand cleavage reported here proceeds with much greater efficiency: it represents ∼43% of all DNA damage initiated at the primary attack site. It may be noted that the experimental protocol employed here obviated the need for the above assumption in the analysis of the experimental data. The observed difference in efficiencies of double-strand cleavage is fully consistent with the geometrical models required to account for these cleavage events. The model presented here allows easy accessibility by the metal center to both cleavable residues; this disposition should facilitate double-strand cleavage. Conversely, previous models require significant geometric rearrangement during the cleavage process to allow access by the metal center to both target hydrogens. Such a requirement would likely lessen the efficiency of double-stranded cleavage relative to the example provided here.

It should be noted that the assignment of C_{31} as the primary cleavage site is based upon the precedent of work from the Povirk laboratory[10,40] and on the quantitative biochemical analyses carried out here. The model derived from NMR measurements and molecular dynamics calculations provides no structural basis for this assignment. Additionally, although the results reported here can be generally considered within the framework of the double-strand cleavage hypothesis put forth by others, some differences do exist. All previously reported double-strand cleavage sites involve nucleotides that are either directly base-paired or are one base pair removed. In contrast, the cleavage presented in this work involves nucleotides that are staggered by three base pairs. Clearly the present model is simpler from a geometric perspective, as no rearrangement of the Fe(II)·BLM−DNA complex[11b,41] need be invoked to provide a structural basis for double-strand cleavage. The molecular modeling studies carried out here fail to define a single, preferred orientation for the bithiazole moiety in its association with the Dickerson−Drew dodecamer. Further, the modeling studies argue that the precise orientation of this portion of the BLM molecule may be unimportant to the observed double-strand cleavage event. The simplicity of the BLM−DNA complex leading to double-strand cleavage distinguishes this work from previous reports. Nonetheless, and perhaps surprisingly, such a configuration of cleaved residues has not been reported previously. The hypothesis of Povirk also stated that cleavage at the secondary site occurred only when coupled to events at the primary site.[10b] The observation of small amounts of single-strand cleavage at both the A_5 and C_{31} sites indicates that, for the duplexes described in this work, hydrogen atom abstraction can be initiated at either site. The detailed mechanistic studies of Absalon et al. have also provided for this possibility.[11b]

Conclusions

Presented herein is a complete chemical characterization of BLM-mediated double-strand DNA cleavage that is fully supported by structural data. The model that has evolved from this work addresses many of the questions that have remained unanswered concerning double-strand cleavage mediated by BLM. It defines an efficient double-strand DNA cleavage site that is easily modeled structurally. Aside from the novel geometry of the cleavage sites in the present study, the model presented is consistent with the chemical mechanism of double-strand cleavage proposed previously.[10,11,40]

Experimental Section

Materials. Fractionation of blenoxane,[44] obtained from Bristol-Myers Squibb Pharmaceuticals, afforded bleomycin A_2, which was further purified by C_{18} reversed-phase HPLC using methanol−ammonium bicarbonate mobile phases. Fe(II)$(NH_4)_2(SO_4)_2$ was purchased from Alfa Biochemicals. Piperidine, sodium borohydride, and *n*-butylamine were purchased from Aldrich Chemical Co. Piperidine was distilled under diminished pressure and stored at −20 °C. All oligonucleotides were either synthesized on a Biosearch 8600 DNA synthesizer using phosphoramidite chemistry[45] or purchased from Cruachem, Inc. They were purified either by C_{18} reversed-phase HPLC (Vydac column 218TP1010 with aqueous ammonium acetate−acetonitrile mobile phases) or preparative denaturing polyacrylamide gel electrophoresis (PAGE) prior to use. [γ-^{32}P]ATP (7000 Ci/mmol) and cordycepin (3000 Ci/mmol) were purchased from ICN Biomedicals. DNase I was purchased from Promega, snake venom phosphodiesterase was from United States Biochemicals, nuclease P1 was from Bethesda Research Laboratories, and calf intenstinal phosphatase was from Boehringer Mannheim Biochemicals. T4 polynucleotide kinase and terminal deoxynucleotidyl transferase were obtained from New England Biolabs. 5′ and 3′-^{32}P end labeling of the oligonucleotides was effected using these enzymes as described.[46] The radiolabeled oligonucleotides were then purified by preparative denaturing PAGE. Maxam−Gilbert sequence analysis was carried out essentially as described.[47] Fe·BLM-mediated DNA oligonucleotide cleavage was carried out as described.[48]

NMR Sample Preparation. NMR studies were carried out using a Zn·BLM A_2 complex, which was prepared by dissolving BLM A_2 in 400 μL of water to a concentration of 5 mM (determined spectropho-

(44) Oppenheimer, N. J.; Rodriquez, L. O.; Hecht, S. M. *Proc. Natl. Acad. Sci. U.S.A.* **1979**, *76*, 5616−5620.
(45) Matteucci, M. D.; Caruthers, M. H. *J. Am. Chem. Soc.* **1981**, *103*, 3185−3191.
(46) (a) Kane, S. A.; Hecht, S. M.; Sun, J.-S.; Garestier, T.; Hélène, C. *Biochemistry* **1995**, *34*, 16715−16724. (b) Tu, C.-P. D.; Cohen, S. N. *Gene* **1980**, *10*, 177−183.
(47) (a) Banaszuk, A. M.; Deugau, K. V.; Sherwood, J.; Michalak, M.; Glick, B. R. *Anal. Biochem.* **1983**, *128*, 281−286. (b) Sambrook, J.; Fritsch, E. F.; Maniatis, T. *Molecular Cloning, A Laboratory Approach;* 2nd ed.; Cold Spring Harbor Laboratory Press: New York, 1989; Vol. 2, p 13.11.
(48) Hamamichi, N.; Natrajan, A.; Hecht, S. M. *J. Am. Chem. Soc.* **1992**, *114*, 6278−6291.

tometrically, ϵ_{292} 14 500 M^{-1} cm^{-1}), followed by the addition of 1 mol equiv of $ZnSO_4$ from a 0.2 M stock solution. The pH of the solution was adjusted to 7.0 using 0.1 M NaOH. This Zn·BLM solution was then added to 1 mol equiv of the dodecanucleotide duplex (determined spectrophotometrically; $\epsilon_{260}1.1 \times 10^5$ M^{-1} cm^{-1} per strand) to afford a 5 mM solution of the drug−DNA complex. For spectra acquired in D_2O, the sample was lyophilized three times from 99.9% D_2O, then redissolved in 100% D_2O.

NMR Experiments. One and two-dimensional ^1H NMR experiments were carried out on a General Electric Omega 500 spectrometer operating at 500.13 MHz, using external TSP (3-(trimethylsilyl)-propionic acid) as a reference. One-dimensional NOE enhancement experiments were performed in 90% H_2O with a 1:1 jump and return pulse sequence[49] for solvent suppression and a sweep width of 10 000 Hz. For two-dimensional experiments, the H_2O resonance was suppressed by continuous wave irradiation for 1.5 s at a sweep width of 5000 Hz. NMR data were processed using the program Felix (Biosym Technologies, San Diego, CA), running on a Silicon Graphics Iris Crimson Elan workstation. The DQF-COSY spectra[50] contained 512 and 2048 complex points in the t_1 and t_2 dimensions, respectively. Initial processing included apodization in both dimensions with a sine squared function shifted by 45° and zero filling to 1024 points in the t_1 dimension. NOESY spectra were obtained at mixing times (τ_{mix}) of 50, 100, and 300 ms. A composite pulse (90_x, 180_y, 90_x) in the middle of the mixing period improved solvent suppression. Homospoil pulses of 5 ms were used at the beginning of τ_{mix} and after the composite 180° pulse.[51] The NOESY spectra consisted of 512 and 2048 complex points in the t_1 and t_2 dimensions, respectively; the spectra were apodized with a 3 Hz exponential in t_1 and a 90° shifted sine bell in t_2. The t_1 dimension was zero-filled to 1024 points. All spectra were acquired with 64 scans of each of the 1024 or 512 t_1 values.

Analysis of the NMR Data. Resonance assignments of Zn·BLM A_2 and the dodecanucleotide $d(CGCGAATTCGCG)_2$ were derived from assessment of the DQF-COSY and NOESY ^1H NMR experiments. With the exception of minor variations in chemical shifts due to temperature and solvent composition, resonances for both Zn·BLM A_2[18] and $d(CGCGAATTCGCG)_2$[14c,d,17] were in agreement with those reported previously. In the BLM-DNA complexes, inter- and intramolecular NOESY cross-peak volumes were converted to interproton distances using the two spin approximation ($r_{ij} = r_{ref}(R_{ref}/R_{ij})^{1/6}$), with the cytidine H5−H6 distance of 2.45 Å used for calibration (r_{ref}).[52] Intramolecular BLM−BLM and DNA−DNA distances were obtained from the NOESY spectra obtained at a mixing time of 100 ms and were classified semiquantitatively into three categories: strong (1.80−2.50 Å), medium (2.51−3.70 Å), and weak (3.71−5.00 Å). The intermolecular BLM−DNA distances were determined from the 300 ms mixing time NOESY spectra and were given a wider range (2.0−5.0 Å) due to the uncertainty in the derived distances. For methyl and methylene protons, another 1 Å was added to the upper bound of the restraints to compensate for center averaging. Qualitative estimation of the pseudorotation angle ranges for the deoxyribose sugars of the dodecanucleotide were obtained from the DQF-COSY spectra.[53]

DNA Restraints. In addition to the experimentally derived distance and dihedral angle restraints obtained from the NMR data, four other types of restraints were used in calculating the structures presented in this study. To preserve the right-handed character of the DNA duplex during the molecular dynamics calculations, the α, β, γ, ϵ, and ξ backbone torsion angles were restrained to a range that covered both right-handed A- and B-DNA.[54] To avoid collapse of the major groove during the high-temperature dynamics phase of the simulation, C1′ atoms on opposite sides of the major groove were restrained to be greater than 16 Å apart.[55] Base pairs were kept Watson−Crick hydrogen bonded by using distance restraints between the bases.[54b] Base pair deviations from coplanarity were constrained by applying dihedral angle restraints. In all, during the modeling of the Zn·BLM A_2−$d(CGCGAATTCGCG)_2$ complex, 12 intermolecular BLM−DNA NOE restraints, 12 nonvicinal BLM−BLM NOE restraints, 250 nonvicinal DNA−DNA NOE restraints, 52 DNA−DNA distance restraints, 243 DNA−DNA dihedral angle restraints, and 19 BLM chiral restraints were utilized. Listings of DNA backbone angle restraints and hydrogen bond distance restraints are available as Supporting Information (Tables 3 and 4, respectively).

Molecular Modeling. Modeling of the interaction of Zn(II)·BLM A_2 with the dodecanucleotide $d(CGCGAATTCGCG)_2$ was performed using the Insight II/Discover program and the Biosym CVFF force field. To model the BLM−metal ion interaction, five-coordinate heme parameters within Insight II were utilized. The metal ion was attached to the secondary amine of Ala, the ring nitrogen of Pyr, the amide and ring nitrogens of His, and the carbamoyl nitrogen of Man (Figure 1). The starting dodecamer duplex structure was constructed in a standard B-form using Insight II. To provide a starting structure of the BLM−DNA complex, the BLM was docked into the minor groove of the B-form dodecamer using the simulated annealing protocol[56] that included the BLM−DNA and BLM−BLM distance restraints. The B-form dodecamer was restrained during the annealing using a template force constant of 10 000 kcal/Å. The resulting structure was utilized as a starting point for the restrained molecular dynamics calculations.

The protocol of restrained dynamics was similar to the one described previously.[12] The starting BLM−DNA structure was first energy minimized with 100 steps of steepest descents, followed by 500 cycles of conjugate gradient minimization with k_{NOE} set at 0.5 kcal·mol^{-1}·$Å^{-2}$ and k_{CDIH} (dihedral restraint constant) set at 5.0 kcal·mol^{-1}·rad^{-2}. The system was then slowly heated to 1000 K. During this high-temperature phase of the simulation, k_{CDIH} was held constant at 50 kcal·mol^{-1}·rad^{-2}, k_{NOE} was slowly increased from 0.5 to 25 kcal·mol^{-1}·$Å^{-2}$, and the relative weights of all force field energy terms were reduced to 25%. The system was then gradually cooled to 300 K and the weights of the force field energy terms were restored to full scale. For the annealing, the dynamics integration time step was 1 fs, the cutoff distance for the nonbonded interactions was set at 10 Å with a switching distance of 2 Å, and a distance-dependent dielectric of $\epsilon = r_{ij}$ was used. The final structures were energy minimized using 30 000 cycles of conjugate gradient minimization to a final root-mean-square derivative of <0.001 kcal·mol^{-1}·$Å^{-2}$. The effect of solvent was approximated by a distance-dependent dielectric of $\epsilon = 4r_{ij}$ and by reducing the net charge on the phosphate group to −0.32e.[57] A formal charge of 2+ was assigned to the metal ion of BLM; the primary amines were protonated.

Acknowledgment. This work was supported by National Institutes of Health Research Grants CA53913 and CA76297, awarded by the National Cancer Institute. We wish to thank Michael Morgan for the initial experiments defining the sites of cleavage of the Dickerson dodecanucleotide by Fe(II)·BLM. We thank Dr. Jeffrey Ellena for helpful discussions regarding this work, and Benjamin Caldwell for assistance with the preparation of some of the figures.

Supporting Information Available: Characterization of the low mobility product formed from duplex degradation by Fe·BLM, and ^1H NMR characterization of the complex formed between Zn·BLM A_5 and $d(CGCGAATTCGCG)_2$ (PDF). This material is available free of charge via the Internet at http://pubs.acs.org.

JA003795I

(49) Plateau, P.; Guéron, M. *J. Am. Chem. Soc.* **1982**, *104*, 7310−7311.
(50) Piantini, U.; Sorensen, O. W.; Ernst, R. R. *J. Am. Chem. Soc.* **1982**, *104*, 6800−6801.
(51) Blake, P. R.; Park, J. B.; Bryant, F. O.; Aono, S.; Magnuson, J. K.; Eccleston, E.; Howard, J. B.; Summers, M. F.; Adams, M. W. W. *Biochemistry* **1991**, *30*, 10885−10895.
(52) Baleja, J. D.; Moult, J.; Sykes, B. D. *J. Magn. Reson.* **1990**, *87*, 375−384.
(53) Kim, S. G.; Lin, L.; Reid, B. R. *Biochemistry* **1992**, *31*, 3564−3574.
(54) (a) Gronenborn, A. M.; Clore, G. M. *Biochemistry* **1989**, *28*, 5978−5984. (b) Baleja, J. D.; Pon, R. T.; Sykes, B. D. *Biochemistry* **1990**, *29*, 4828−4839.
(55) Huang, P.; Eisenberg, M. *Biochemistry* **1992**, *31*, 6518−6532.
(56) Nilges, M.; Clore, G. M.; Gronenborn, A. M. *FEBS Lett.* **1988**, *229*, 317−324.
(57) Tidor, B.; Irikura, K. K.; Brooks, B. R.; Karplus, M. *J. Biomol. Struct. Dyn.* **1983**, *1*, 231−252.